

Spin structure of diatomic van der Waal molecules of alkali atoms

Jing-Lun Li,¹ Paul S. Julienne,² Johannes Hecker Denschlag,¹ and José P. D’Incao^{3,4}

¹*Institut für Quantenmaterie and Center for Integrated Quantum Science and Technology IQST, Universität Ulm, 89069 Ulm, Germany*

²*Joint Quantum Institute, University of Maryland,*

and the National Institute of Standards and Technology (NIST), College Park, MD 20742, USA

³*JILA, NIST, and the Department of Physics, University of Colorado, Boulder, CO 80309, USA*

⁴*Department of Physics, University of Massachusetts Boston, Boston, MA 02125, USA*

(Dated: November 26, 2024)

We theoretically investigate the spin structure of weakly bound diatomic van der Waals molecules formed by two identical bosonic alkali atoms. Our studies were performed using known Born-Oppenheimer potentials while developing a reduced interaction potential model. Such reduced potential models are currently a key for solving certain classes of few-body problems of atoms as they decrease the numerical burden on the computation. Although the reduced potentials are significantly shallower than actual Born-Oppenheimer potentials, they still capture the main properties of the near-threshold bound states, including their spin structure, and the scattering states over a broad range of magnetic fields. At zero magnetic field, we find that the variation in spin structure across different alkali species originates from the interplay between electronic spin exchange and hyperfine interactions. To characterize this competition we introduce a single parameter, which is a function of the singlet and triplet scattering lengths, the atomic hyperfine splitting constant, and the molecular binding energy. We show that this parameter can be used to classify the spin structure of vdW molecules for each atomic species.

I. INTRODUCTION

Van der Waals (vdW) complexes are weakly bound molecular states held together by long-range dispersion interactions, in contrast to typical molecular states where the strong chemical bond originates from the overlap of the atom’s electron clouds [1, 2]. These fragile molecules play a central role across a broad range of phenomena across physics, chemistry, biology, and materials science [3–7]. Intensive investigations of vdW complexes span from spectroscopy in supersonic molecular beams [8, 9], self-assembly in nanostructures [10–12], molecular dynamics of biopolymers [13, 14], superfluidity of the Helium droplets [15–22], to the controlled formation, manipulation and state-resolved detection of vdW molecules in ultracold quantum gases of alkali metal atoms [5, 23–30].

An important direction of research involving vdW molecules concerns cold, controlled chemical reactions. Recent studies with ultracold atomic gases have revealed that the spin structure of the van der Waals bound state can play an important role in the product distribution following reactions such as three-body recombination [29, 31, 32]. In particular, the specific spin structure of Rb₂ vdW bound states at low magnetic fields gives rise to a spin conservation propensity rule in three-body recombination [29, 30]. One can also expect that similar spin propensity rules exist for cold reactions between vdW molecules colliding with atoms and that they depend on the molecular spin structure. Furthermore, the spin structure of vdW molecules can vary considerably among alkali species and can ultimately influence how they can be manipulated by external fields. Therefore, determining the spin

structure of vdW molecules is of fundamental importance to understand and explore various types of ultracold chemical reactions currently accessible to experiments with ultracold atoms and molecules.

Investigating the spin structure of alkali vdW diatomic molecules can be done by solving the coupled-channel Schrödinger equation with well-known *ab initio* Born-Oppenheimer (BO) potentials [33–37] and hyperfine interactions. However, for future implementation in reaction dynamics in three-body numerical simulations [38] it is also imperative to design simpler potential models to replace the actual BO potentials. In the simplified model, potentials can typically be made much shallower to alleviate the computational burden in three-body calculations [39–41]. We explore this aspect in this present manuscript. Numerical simulations for three-body recombination of ultracold atoms, which use the actual BO potentials, have been conducted in Refs. [31, 42, 43]. However, in such studies, additional high momentum truncations were implemented in momentum-space [31, 42, 43], which has a similar effect to reducing the depth of potential in coordinate space.

In this work, we investigate the vdW molecules of two identical bosonic alkali atoms for ⁷Li, ²³Na, ³⁹K, ⁴¹K, ⁸⁵Rb, ⁸⁷Rb and ¹³³Cs and characterize the spin structure of these molecules states. We find that, at zero magnetic field, the molecular spin structure is determined by the competition between electronic spin exchange and hyperfine interactions. Such competition varies across different species and can be qualitatively described by a single parameter, defined by the singlet and triplet scattering lengths, the atomic hyperfine splitting constant, and the molecular binding energy. We construct reduced potential models for such diatomic

vdW systems that are shallower but largely preserve the major properties of the actual interactions. We aim to design for each species a potential model that is generally good for representing the binding energy and spin structure of weakly bound vdW molecules. We show that the reduced potentials also describe well the low-energy scattering property of two atoms. In fact, we find that the latter criterion can be used as a practical way to construct the reduced potential so that the former criterion is automatically satisfied. The rest of this paper is organized as follows: in Section II we introduce our theoretical framework, characterize the range of binding energies where the molecular states can be considered as vdW molecules and detail our procedure to construct reduced model potentials. In Section III we compare the results of reduced and realistic potentials. We characterize the spin mixing of vdW molecules in Section IV and summarize our main findings and conclusion in Section V.

II. THEORETICAL FRAMEWORK

For two alkali atoms in an external magnetic field the Hamiltonian reads

$$\hat{H} = \hat{T}(r) + \hat{V}(r) + \hat{H}_{\text{hf}} + \hat{H}_Z, \quad (1)$$

where \hat{T} and \hat{V} denote the kinetic and potential energy operators, respectively, and r is the interatomic distance. The third term above represents the sum of the two (identical) atomic hyperfine interactions, $\hat{H}_{\text{hf}} = A_{\text{hf}}(\vec{s}_a \cdot \vec{i}_a)/\hbar^2 + A_{\text{hf}}(\vec{s}_b \cdot \vec{i}_b)/\hbar^2$, where A_{hf} is the hyperfine constant, and \vec{s}_i and \vec{i}_i the electronic and nuclear spins, respectively, of atom i ($i = a, b$). The fourth term describes the Zeeman Hamiltonian $\hat{H}_Z = (\gamma_e \vec{s}_a + \gamma_n \vec{s}_b - \gamma_n \vec{i}_a - \gamma_n \vec{i}_b) \cdot \vec{B}$ in the presence of a homogeneous magnetic field in the \hat{z} , $\vec{B} = B\hat{z}$, with γ_e and γ_n being the electronic and nuclear gyromagnetic factors, respectively. The physical parameters for the alkali atoms discussed above can be found in Ref. [44]

In our calculations we neglect higher-order terms in the Hamiltonian [Eq. (1)] associated with magnetic dipolar interactions as they typically introduce only a small effect [45]. As a result, we can write the total wave function $\Psi(\vec{r})$ as

$$\Psi(\vec{r}) = \sum_{\alpha} \frac{\psi_{\alpha}(r)}{r} Y_{lm_l}(\theta, \phi) |\alpha\rangle, \quad (2)$$

where Y_{lm_l} is the spherical harmonics for the orbital angular moment l and azimuthal projection m_l , $|\alpha\rangle$ is the eigenstate of $\hat{H}_{\text{hf}} + \hat{H}_Z$ with eigenvalue E_{α} , and $\psi_{\alpha}(r)$ is the radial wavefunction. At zero magnetic field, $|\alpha\rangle = |f_a m_{f_a}\rangle |f_b m_{f_b}\rangle$ is the direct product of the eigenstates $|f m_f\rangle$ of the atomic hyperfine spins ($\vec{f} = \vec{s} + \vec{i}$) where f is the hyperfine spin and m_f its azimuthal projection. Note that here we will use $|f_a m_{f_a}\rangle |f_b m_{f_b}\rangle$ to label $|\alpha\rangle$ states

even when a magnetic field is non-zero. At each magnetic field B , we then solve the coupled channel Schrödinger equation given by

$$\left[-\frac{\hbar^2}{m} \frac{d^2}{dr^2} + \frac{l(l+1)}{mr} \hbar^2 + E_{\alpha} \right] \psi_{\alpha}(r) + \sum_{\alpha'} \langle \alpha | \hat{V}(r) | \alpha' \rangle \psi_{\alpha'}(r) = E \psi_{\alpha}(r), \quad (3)$$

where m is the atomic mass. For alkali atoms, the interatomic interactions depend on the electronic spins and we represent the potential energy operator as

$$\hat{V}(r) = \sum_{SM_S} |SM_S\rangle V_S(r) \langle SM_S|, \quad (4)$$

where S is the total electronic spin, $|s_a - s_b| \leq S \leq s_a + s_b$, and $-S \leq M_S \leq S$ is azimuthal projection. For alkali atoms the electronic spins allow for the singlet (s), $S = 0$, and triplet (t), $S = 1$, BO interactions. We use $S = 0$ or 1, and s or t interchangeably as indices in the following. For all species considered in this study, the actual BO potentials of two identical atoms are considerably deep, typically supporting ~ 10 to ~ 100 s -wave ($l = 0$) bound states [33–37], with a total number of rovibrational states ranging from hundreds up to a few thousands. Our calculations show that the least number of the s -wave bound states is 11, arising from the triplet potential of ${}^7\text{Li}_2$ while the highest number is 156 from the singlet potential of ${}^{133}\text{Cs}_2$. Figure 1 shows the BO potentials (taken from Ref. [33]) and the s -wave bound levels of ${}^7\text{Li}_2$ to illustrate their general form. The two potentials deviate at short range due to electronic spin-exchange interactions but become nearly identical beyond a critical internuclear distance, r_{ex} , which will be defined in the following. The dominant contribution to the long-range part of the BO potentials is given by the $-C_6/r^6$ dispersion interaction. Here, C_6 is the vdW dispersion coefficient, from which we define the characteristic length $r_{\text{vdW}} = (mC_6/\hbar^2)^{1/4}/2$ and energy $E_{\text{vdW}} = \hbar^2/mr_{\text{vdW}}^2$ scales of the vdW interaction. These two vdW characteristic scales, r_{vdW} and E_{vdW} , define a units system that provides a unified framework for describing all atomic species. We will use vdW units throughout the following discussion unless otherwise specified.

A. Criteria for vdW molecular states

As we mentioned above, vdW molecules are weakly bound molecular states held together by long-range dispersion interactions. For such molecular states, the electronic cloud for each of the atoms have little to none overlap, making vdW molecules fundamentally different to typical molecular states where the strong chemical bound originates from the overlap of the electronic clouds [1, 2]. In order to characterize the range of binding energies for vdW molecules, we can estimate

TABLE I. Parameters for classifying vdW molecules composed of two identical bosonic alkali atoms

Molecule	r_{vdW}/a_0	$r_{\text{ex}}/r_{\text{vdW}}$	r_{ex}/a_0	E_{vdW}/h [MHz]	$E_s^{\text{max}}/E_{\text{vdW}}$	$E_t^{\text{max}}/E_{\text{vdW}}$	E_s^{max}/h [THz]	E_t^{max}/h [THz]
${}^7\text{Li}_2$	32.49	0.4583	14.89	487.48	2617	2141	1.28	1.04
${}^{23}\text{Na}_2$	44.96	0.3483	15.66	77.67	14105	11538	1.10	0.90
${}^{39}\text{K}_2$	64.61	0.2703	17.46	22.19	67097	54911	1.49	1.22
${}^{41}\text{K}_2$	65.42	0.2669	17.46	20.59	72405	59242	1.49	1.22
${}^{85}\text{Rb}_2$	82.16	0.2189	17.99	6.30	245495	200822	1.54	1.26
${}^{87}\text{Rb}_2$	82.64	0.2177	17.99	6.08	253623	207567	1.54	1.26
${}^{133}\text{Cs}_2$	101.07	0.1863	18.82	2.66	661003	540800	1.76	1.44

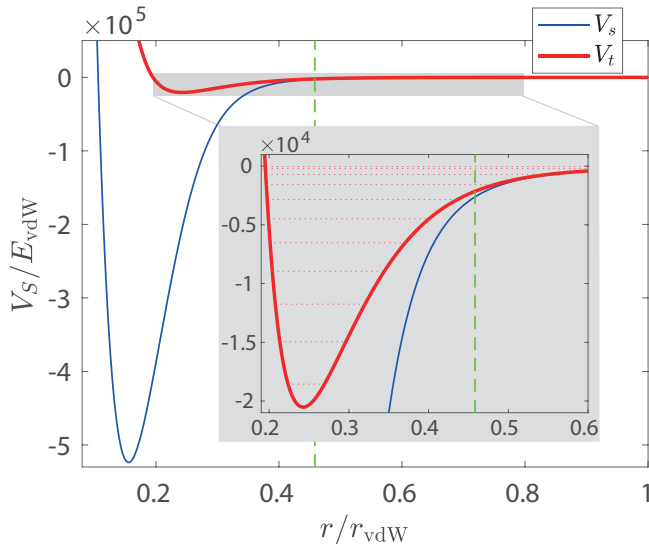


FIG. 1. Singlet (thin blue) and triplet (thick red) BO potentials of ${}^7\text{Li}_2$ are displayed in vdW units. The vertical dashed line represents a critical internuclear distance, r_{ex} , defined in the text for classifying the vdW molecules. The inset provides a zoomed-in view of the shaded region, showing 11 triplet s-wave bound levels marked by dotted lines.

the dominant role of the vdW interaction at different interatomic distances, thus allowing us to estimate the size (and energy) of the molecular states where vdW interactions prevails over the electronic exchange. The dominance of the vdW interaction can be roughly estimated via the ratio

$$\sigma_{\text{ex}}(r) \equiv \frac{V_{\text{vdW}}(r)}{V_{\text{ex}}(r)} = \frac{V_s(r) + V_t(r)}{V_s(r) - V_t(r)} \quad (5)$$

by assuming $V_{s/t} \approx V_{\text{vdW}} \pm V_{\text{ex}}$, where V_{ex} and V_{vdW} denote the electronic spin-exchange interaction and the vdW interaction respectively. We define the critical internuclear distance r_{ex} by setting $\sigma_{\text{ex}}(r_{\text{ex}}) = 10$, ensuring that $V_{\text{vdW}} \gg V_{\text{ex}}$ when $r \geq r_{\text{ex}}$. The dominance of vdW interaction at $r \geq r_{\text{ex}}$ is demonstrated in Fig. 1, using ${}^7\text{Li}_2$ as an example (see Table I for the corresponding values of r_{ex} .) Accordingly, a molecule can be classified as a vdW molecule if its size exceeds r_{ex} or, equivalently, its binding energy is smaller than the

critical value defined as $E_S^{\text{max}} \equiv |V_S(r_{\text{ex}})|$. The critical values for the molecular binding energies are listed in Table I. We find that the E_s^{max} and E_t^{max} are typically around 1 THz, corresponding to a r_{ex} of approximately 15-19 a_0 . Nevertheless, as we can see from Table I, ${}^7\text{Li}$ is the atomic species with the most restrictive range of binding energies in vdW units, with a critical value of a few thousand E_{vdW} . Therefore, in this work, we will only consider molecular states with a binding range of up to a few thousand E_{vdW} to ensure that the vdW interaction dominates molecular bond formation for all species explored.

B. Constructing reduced potential models

This section aims at introducing a reduced interaction model to replace V_S in Eq. (4), containing a much smaller number of molecular states and denoted by V_S^* . Both reduced singlet V_s^* and triplet V_t^* potentials should be sufficiently shallower than their originals and reproduce well the low-energy bound and scattering properties of the system. Here, we define the reduced potentials as

$$V_S^*(r) = V_S(r) + \frac{C_6 \lambda_S^6}{r^{12}}, \quad (6)$$

where V_S is the actual BO potential and λ_S is a free (length) parameter used to tune the introduced short-range $1/r^{12}$ repulsion. This effectively reduces the number of bound states.

Our reduced potentials are determined by tuning λ_S to the values of λ_s and λ_t that reproduce the values of the singlet a_s and triplet a_t scattering lengths, respectively, obtained from the corresponding BO potentials [33–37]. [Values of a_s and a_t were calculated by simply setting $E_\alpha = 0$ and $\hat{V} = V_{s/t}$ or $V_{s/t}^*$ in Eq. (3).] Evidently, there are multiple choices of λ_s and λ_t that reproduce the values of a_s and a_t , each corresponding to a different number of s-wave bound states that the reduced potentials can support. For our present study, we choose the number of s-wave singlet states to be $n_s = 6$, except for ${}^{133}\text{Cs}$, where we choose $n_s = 7$ (see later discussion). For the reduced triplet interaction, this number is chosen as $n_t = n_s$ for cases where $a_s < a_t$, or

TABLE II. Parameters for the reduced potentials, $n_{s/t}$, $\lambda_{s/t}$, $\lambda_{s/t}^*$, and c_{hf} (see text), along with the relevant parameters characterizing the corresponding atomic species, $a_{s/t}$ and A_{hf} . See Table I for the corresponding values of r_{vdW} . Note that here we list A_{hf} with only two decimal places, while in our calculation the precise value from Ref. [44] is employed.

Molecule	a_s/a_0	n_s	λ_s/r_{vdW}	$\lambda_s^*/r_{\text{vdW}}$	a_t/a_0	n_t	λ_t/r_{vdW}	$\lambda_t^*/r_{\text{vdW}}$	A_{hf}/h [MHz]	c_{hf}
$^7\text{Li}_2$	34.34	6	0.3792958	λ_s	-26.85	5	0.3181707	λ_t	200.88	1
$^{23}\text{Na}_2$	18.83	6	0.3395979	λ_s	64.31	6	0.3235117	λ_t	442.91	1
$^{39}\text{K}_2$	138.89	6	0.3272250	0.3269770	-33.28	5	0.3354390	0.3354690	115.43	1
$^{41}\text{K}_2$	85.43	6	0.3226359	0.3225499	60.29	5	0.3437314	0.3437234	63.50	1
$^{85}\text{Rb}_2$	2654.70	6	0.3242030	λ_s	-389.63	5	0.3257500	0.3258900	505.96	0.9477
$^{87}\text{Rb}_2$	90.20	6	0.3131870	0.3133710	98.91	6	0.3138290	0.3140510	1708.67	0.9026
$^{133}\text{Cs}_2$	286.52	7	0.2946725	0.2896405	2857.28	7	0.2974180	0.2993080	1149.08	0.8710

$n_t = n_s - 1$ for cases where $a_s > a_t$. This ensures that the singlet potential is deeper than the triplet potential in the reduced potential model, consistent with the actual BO potentials. According to our analysis in Section IIA, all the levels included in the reduced potentials are vdW molecules except for the last two singlet and the last triplet $^7\text{Li}_2$ levels. Including deeper bound state levels, particularly for ^7Li , is beyond the scope of the present work as the vdW interaction may no longer be dominant in a molecular bond formation. The values of λ_s and λ_t , and corresponding scattering lengths are listed in Table II.

Figure 2 (upper panel) compares the energies of the first few singlet and triplet bound state levels, E_s and E_t , respectively, of the reduced potentials (dashed lines) to those obtained from the original BO potentials (solid lines). The figure shows that by matching the singlet and triplet scattering lengths one obtains a very good agreement between the energy levels to the results from BO potentials. Evidently, such agreement deteriorates for more deeply bound levels as shown in the lower panel of Fig. 2. Such deterioration originates from the fact that the reduced potentials are much shallower than the BO potentials. This can be further improved by using deeper reduced models containing a larger number of molecular states. Figure 2 also clearly shows that each colored block contains exactly one bound level for each potential (note that the levels in the energy range of [-600, -300] E_{vdW} are not shown due to a break in the y-axis). As we shall discuss in more detail later in Section IV, these colored blocks represent a universal structure of the dimer spectrum of vdW potentials, conventionally referred to as the vdW energy bins [45, 46].

Throughout this work, we use the log-derivative algorithm [47] to solve the Schrödinger equation (3) for calculating the low-energy scattering quantities. We switch to a mapped grid Hamiltonian method [48] when bound level energies or the scattering and bound state wavefunctions are required.

III. PERFORMANCE OF THE REDUCED POTENTIALS

Although we find that the reduced singlet and triplet potentials reproduce well the molecular energies, for applications in ultracold atoms the actual performance of the reduced potential model needs to be reevaluated in the presence of hyperfine and Zeeman interactions, \hat{H}_{hf} and \hat{H}_Z in Eq. (1). In fact, we find that the reduced potentials need to be fine-tuned to precisely describe the low energy scattering properties of the system at finite B -fields for some species. In this section, we describe such adjustments and evaluate the performance of the reduced potentials in comparison to the BO potentials by analyzing the corresponding scattering and bound properties as well as the spin structure of both scattering and molecular states.

A. Scattering properties

For our present study, we consider that the colliding atoms are prepared in the hyperfine spin-stretched state, $|f=f_*, m_f=-f_*\rangle$, of the lowest hyperfine manifold. Concretely, $f_* = 3$ for ^{133}Cs , $f_* = 2$ for ^{85}Rb and $f_* = 1$ for all other atomic species. We focus on the low magnetic field range of [-200, 200] G, which is the typical accessible experimental regime of Refs. [27–30] and for many other experiments. We note that considering the $|f=f_*, m_f=-f_*\rangle$ state at a negative magnetic field is equivalent to studying the physics of the $|f=f_*, m_f=+f_*\rangle$ state at $|B|$. Since the reduced models obtained in the previous section do not include the effects of hyperfine and Zeeman interactions further adjustments might be necessary to better fit the B -field dependency of the relevant physical observables. Here, we choose to use the low energy scattering properties of the system, parameterized by the s -wave scattering length $a(B)$ and effective range $r_e(B)$, to establish such adjustments. At each B -field, we solve the radial coupled channel Schrödinger equation (3) while varying the collision energy, E . By determining the energy-dependent phase shift $\delta(k)$, where $k = \sqrt{mE}/\hbar$, we extract $a(B)$ and $r_e(B)$ from the effective range

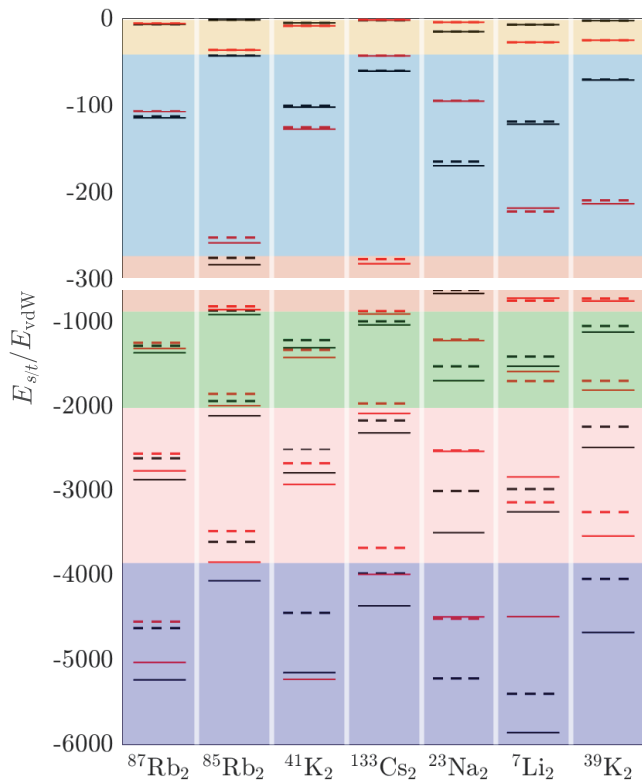


FIG. 2. Singlet E_s (black) and triplet E_t (red) molecular energies from the BO potentials (solid lines) and from the corresponding reduced (dashed lines) potentials (see Table II) for bosonic alkali dimers. The alkali species are arranged in order of increasing effective singlet-triplet level splitting u_{st} . The colored regions represent different ‘energy bins’. Both u_{st} and ‘energy bin’ are defined later in Section IV A. The upper panel highlights the most weakly bound molecular states displaying a good agreement between the energies from the BO and reduced potentials. This agreement deteriorates for the more deeply bound molecular states displayed in the lower panel.

expansion

$$k \cot \delta(k) = -\frac{1}{a} + \frac{1}{2}r_e k^2 + \mathcal{O}(k^4). \quad (7)$$

In order to precisely reproduce the values of $a(B)$ and $r_e(B)$ obtained from the BO potentials, we allow for small variations the values of $\lambda_s \rightarrow \lambda_s^*$ and $\lambda_t \rightarrow \lambda_t^*$ controlling the reduced potentials [Eq. (6)]. In addition to that, for heavier atomic species where the hyperfine splitting constant is typically large, we will also allow for slight changes the value of the hyperfine constant A_{hf} in Eq. (1). This new hyperfine constant is given by $A_{\text{hf}}^* = c_{\text{hf}} A_{\text{hf}}$, where c_{hf} should be kept close to 1 to preserve the main spin structure of the system.

The resulting performance of reduced potentials in describing the magnetic field-dependent scattering properties is demonstrated in Figs. 3 and 4 for the adjusted model parameters $\lambda_{s/t}^*$ and c_{hf} listed in Table. II.

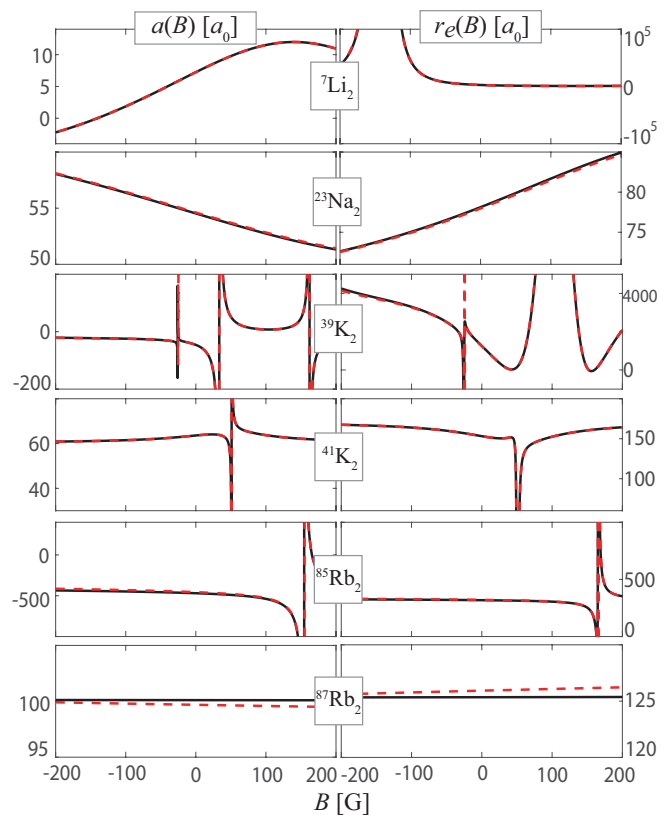


FIG. 3. Scattering length $a(B)$ and effective range $r_e(B)$ of two identical bosonic alkali atoms from original (solid lines) and reduced potentials (dashed lines). It should be noted that we use $|f^*, m_f = -f^*\rangle$ as the reference spin state for the whole considered magnetic field range, which means that a negative magnetic field value represents the $|f^*, m_f = f^*\rangle$ state at $|B|$.

For all species, the $a(B)$ and $r_e(B)$ are very well reproduced by the reduced potentials in $[-200, 200]$ G, as compared to the result from the original BO potentials. Remarkably, the features of the Feshbach resonances and the zero crossing of $a(B)$ [or equivalently, the divergence of $r_e(B)$] in ${}^7\text{Li}_2$, ${}^{39}\text{K}_2$, ${}^{41}\text{K}_2$ and ${}^{85}\text{Rb}_2$ are correctly captured (see Fig. 3). These features are important ingredients for investigating three-body problems regarding, for instance, the Efimov effect [40, 42, 49, 50] and the control of three-body reaction via a magnetic field [51]. To achieve such a good agreement, fine-tuning in λ_s and λ_t is either not necessary (as for ${}^7\text{Li}_2$ and ${}^{23}\text{Na}_2$, and the singlet potential of ${}^{85}\text{Rb}_2$), or required to less than 0.1%. The hyperfine constant is reduced by about 5% and 10% for ${}^{85}\text{Rb}_2$ and ${}^{87}\text{Rb}_2$, respectively. As a result, the number of s -wave bound states, n_s and n_t , is not affected while shifts in the molecular energies (compared to those in Fig. 2) and in a_s and a_t (if any) are typically within a few percent.

The adjustment of parameters for the heaviest atomic species ${}^{133}\text{Cs}$ (see Fig. 4) is slightly different. The low B -field scattering properties of ${}^{133}\text{Cs}_2$ in $|f_* m_f^*\rangle |f_* m_f^*\rangle$ state are strongly affected by multiple Feshbach resonances.

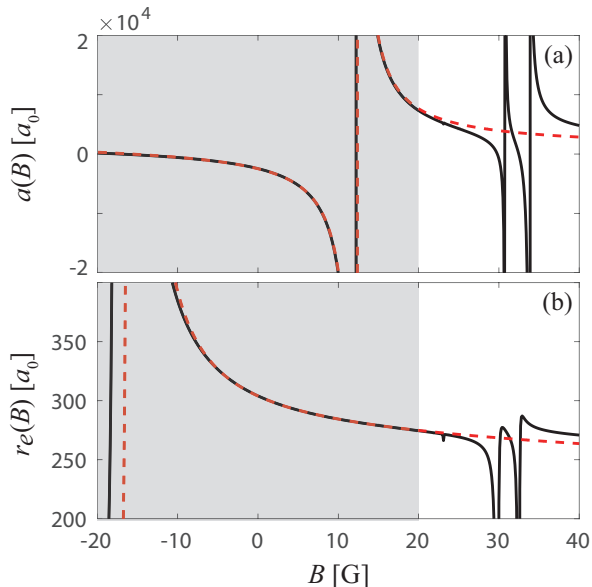


FIG. 4. The s -wave two-body scattering length (a) and effective range (b) for $^{133}\text{Cs}_2$ from the original potentials (solid line) and reduced potentials (dashed line). For the calculation with original potentials we include the dipole-dipole interaction and take both the s and d partial wave into account, while for that with reduced potentials, we neglect the dipole-dipole interaction. The shaded area indicates the considered magnetic field regime for fine-tuning λ_s and λ_t . It should also be noted that we use $|f^*, m_f^* = -f^*\rangle$ as the reference spin state for the whole considered magnetic field range, which means that a negative magnetic field value represents the $|f^*, m_f = f^*\rangle$ state at $|B|$.

We emphasize that the first resonance at $B = 12$ G originates from an s -wave molecular state. In addition, there are resonances at $B = 31$ G and 33 G caused by a d -wave molecular level crossing the s -wave threshold. The latter resonances occur due to the couplings from the magnetic dipole-dipole interaction [37]. As a result, a thorough theoretical model for $^{133}\text{Cs}_2$ would need to incorporate the magnetic dipole-dipole interaction into Hamiltonian (1) in order to allow for the coupling between s and d partial waves. This would add a significant degree of complexity in both two- and three-body numerical simulations [52, 53]. Since our goal is to develop a simple reduced potential model for further uses in three-body calculations, we include the magnetic dipole-dipole interaction for ^{133}Cs only when we calculate $a(B)$ and $r_e(B)$ from the BO potentials and adjust the reduced potentials to fit these results. As a result, we only accurately reproduce the s -wave resonance at $B = 12$ G. This resonance is caused by a $v = -7$ closed-channel bound level crossing the open-channel threshold. It is crucial to include this level in the reduced potentials to

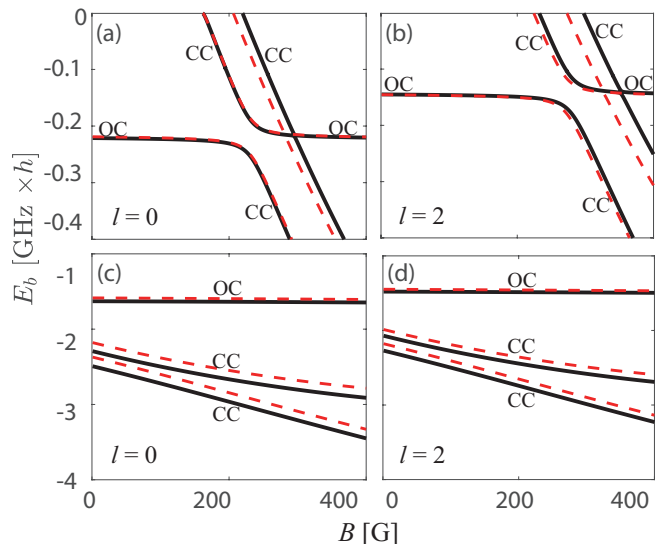


FIG. 5. The energy of s -wave, (a) and (c), and d -wave, (b) and (d), molecular levels of $^{85}\text{Rb}_2$ obtained from the original potentials (solid lines) and reduced potentials (dashed lines). We use ‘OC’ or ‘CC’ to indicate that the molecular level belongs to the incoming open channel or a closed channel, respectively. Note that such a classification does not apply in the vicinity of an avoid crossing.

properly capture the resonance feature. Therefore, we use a larger number of bound states, i.e., $n_s = 7$, for $^{133}\text{Cs}_2$ than other species. Since our reduced potential model can not describe the d -wave resonances at 31 G and 33 G, the fitting should also avoid the corresponding magnetic field regime. We fine-tune the short-range potential parameters, λ_s and λ_t , to fit the reference values of $a(B)$ and $r_e(B)$ in the range of $[-20, 20]$ G for $^{133}\text{Cs}_2$, with c_{hf} also being adjusted (see Table II). Figure 4 shows the good performance of our obtained reduced potential in reproducing the physical $a(B)$ and $r_e(B)$ in this magnetic field regime. However, in the range of $[20, 40]$ G, the result of the reduced potentials deviates from that of the original BO potentials. We note that the fine-tuning of λ_s and λ_t for ^{133}Cs is relatively large ($1\% \sim 2\%$) as compared to other species, leading to $n_s \rightarrow n_s - 1$ while n_t is still unchanged. We attribute this to the omission of dipole-dipole interaction. The reduction of hyperfine constant by c_{hf} is about 13% .

B. Bound state properties

Weakly bound vdW molecules are fragile and highly susceptible to external perturbations. Consequently, an external field, such as a magnetic field, can significantly alter their loose bonds, offering a valuable opportunity to control the properties of these molecules. This subsection examines the response of weakly bound vdW molecular levels to a magnetic field and assesses the performance of the reduced potentials on that. The success of the

reduced potentials in accurately reproducing $a(B)$ and $r_e(B)$ suggests that these potentials are also capable of reproducing the bound levels. Here, we demonstrate this in more detail by using the results obtained for $^{85}\text{Rb}_2$ as an example. In Fig. 5 we compare a group of $l = 0$ and 2 bound level energies obtained from the reduced and BO potentials. For the most weakly bound states [Fig. 5(a) and 5(b)], the corresponding energies for both partial waves are in general well reproduced by our reduced potential in a wide range of B -field [0, 400] G, i.e., even beyond the regime considered in the fitting process discussed in the previous section. As expected, deviations become more perceptible for deeper molecular levels, as shown in Fig. 5(c) and 5(d). In Fig. 5, the molecular levels that are independent of the magnetic field correspond to the incoming channel levels. In contrast, the other molecular levels, which are strongly dependent on the magnetic field, are associated with closed channels. The closed channels have a magnetic moment difference relative to the incoming channel. The magnetic moments of these molecular states, reflected in the slopes of the energy curves, are largely conserved, except when strong couplings between molecular levels occur by chance, such as during an avoided crossing. We shall discuss more details of the avoided crossing in the next subsection. A closed channel molecular state is more deeply bound (by the corresponding threshold separation) than an incoming channel molecular level at the same energy. Consistently, deviations are also more perceptible for the closed channel molecular states in Fig. 5. We note that our reduced potentials can typically support bound states in a partial wave of up to $l = 20$. We have also checked the energies of states of $l > 2$ partial waves and found that the performance of the reduced potential is generally good for small l . We observe similar results for the other atomic species studied here.

C. Spin structure

The spin structure of low-energy scattering and weakly bound vdW molecular states are also expected to respond to an external field, allowing for their manipulation. Given the various spin selection rules and propensity laws that govern molecular reactions, this manipulation offers promising potential for controlling these reactions. We investigate in the following the spin structure of the scattering $|\Psi_{\text{scat}}\rangle$ and molecular $|\Psi_{\text{m}}\rangle$ states of alkali dimers in the presence of a magnetic field and examine the performance of the reduced potential in this context. We first study the spin components of the scattering state. We shall use $^7\text{Li}_2$ at $B = 0$ G as an example, which is particularly relevant for our three-body analysis [32]. For that analysis, we need to introduce two types of molecular spin bases $|FM_F(f_a f_b)\rangle$ and $|FM_F[SI]\rangle$, representing the different ways the atomic spins can be combined. Here, F and I are the quantum numbers of two-atom total spin $\vec{F} = \vec{f}_a + \vec{f}_b$ and total nuclear spin

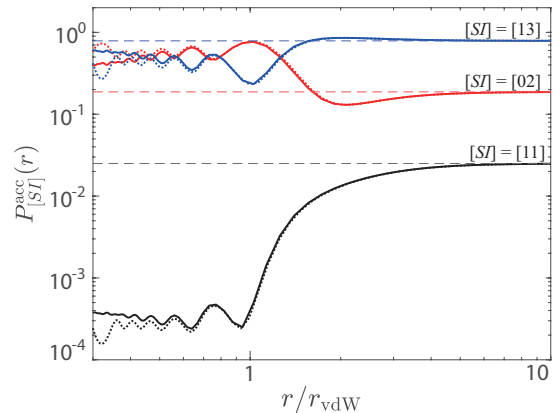


FIG. 6. The accumulated spin fraction $P_{[SI]}^{\text{acc}}$ of the scattering state for $^7\text{Li}_2$ at zero B -field, obtained from the original potentials (solid lines) and reduced potentials (dotted lines). The horizontal dashed lines indicate the spin fraction of 0.1875, 0.0250, and 0.7875 predicted by the basis transformation coefficient.

$\vec{I} = \vec{i}_a + \vec{i}_b$, respectively. The projection quantum number of \vec{F} is denoted as M_F . (Details of the definition and relationship between $|FM_F(f_a f_b)\rangle$ and $|FM_F[SI]\rangle$ spin basis are given in Appendix A.)

Given that both ^7Li atoms are in the $[1, -1]$ state, the spin state of scattering state $|\Psi_{\text{scat}}\rangle$ of $^7\text{Li}_2$ is, at large distances, the $|FM_F(f_a f_b)\rangle = |2-2(11)\rangle$. In contrast, by analyzing the spin structure of the $^7\text{Li}_2$ molecular states $|\Psi_{\text{m}}\rangle$ we have found that most of them can not be represented by a pure $|FM_F(f_a f_b)\rangle$ state, unlike the case for ^{85}Rb and ^{87}Rb atoms, for instance. They are instead well characterized by a single $|FM_F[SI]\rangle$ state. We note that most of the molecular states of $^{23}\text{Na}_2$, $^{39}\text{K}_2$ and $^{41}\text{K}_2$ can also be well characterized by a single $|FM_F[SI]\rangle$ state, while the spin characterization will be more complicated for $^{133}\text{Cs}_2$ (see next section for more details). Therefore, it is valuable to analyze the relationship between the spins of the scattering states and molecular states for ^7Li as a representative example for similar species such as ^{23}Na , ^{39}K and ^{41}K . This relation can play a major role in reaction processes like three-body recombination [29, 32]. As is well known, a $|FM_F(f_a f_b)\rangle$ can be expressed as a linear combination of $|FM_F[SI]\rangle$ states of the same F and M_F . For convenience, this basis transformation relation is presented in Appendix A. As a result, for $^7\text{Li}_2$, the $|FM_F[SI]\rangle$ components $P_{[SI]}$ (explicit definition for $P_{[SI]}$ is given below) of the scattering state in the whole spatial space are $P_{[02]} : P_{[11]} : P_{[13]} = 0.1875 : 0.0250 : 0.7875$. However, as atoms approach interatomic distances $r \sim r_{\text{vdW}}$, the spin structure of the scattering state will change. In fact, a more precise characterization of the spin structure is needed for understanding chemical reactions that typically occur within a finite interparticle volume [29, 32]. Therefore, we define an accumulated

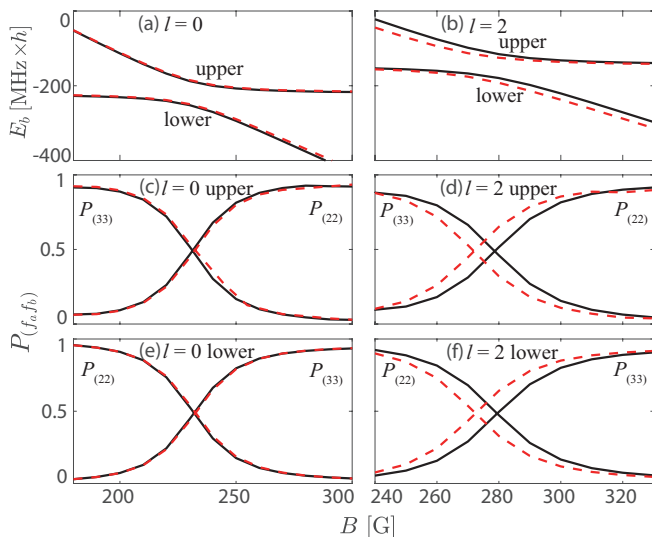


FIG. 7. The energy of the broad s -wave (a) and d -wave (b) avoided crossing levels of $^{85}\text{Rb}_2$. We note that (a) and (b) are zoomed-in views of Figs. 5(a) and 5(b), respectively, with irrelevant levels omitted. (c) and (e) show the $|FM_F(f_a f_b)\rangle$ component, $P_{(f_a f_b)}$, of the upper and lower levels in (a), respectively. (d) and (f) show $P_{(f_a f_b)}$ of the upper and lower levels in (b), respectively. The results are calculated by using the original potentials (solid lines) and reduced potentials (dashed lines).

spin component P_η^{acc}

$$P_\eta^{\text{acc}}(r) \equiv \frac{\int_0^r |\langle FM_F \eta | \Psi(\vec{r}') \rangle|^2 d^3 \vec{r}'}{\sum_{\eta'} \int_0^r |\langle FM_F \eta' | \Psi(\vec{r}') \rangle|^2 d^3 \vec{r}'}, \quad (8)$$

to quantify the spin components of the two-atom state $|\Psi\rangle$ [given by Eq. (2)] within a finite r . Here $|\Psi\rangle$ can be $|\Psi_{\text{scat}}\rangle$ or $|\Psi_{\text{m}}\rangle$ and $\eta = [SI]$ or $(f_a f_b)$. Consequently, the full component P_η is taken at the limit $P_\eta \equiv P_\eta^{\text{acc}}(r \rightarrow \infty)$. Figure 6 shows that the $P_{[SI]}^{\text{acc}}$ calculated from our reduced potentials is in excellent agreement with that calculated from the BO potentials, in particular, when $r > 0.6 r_{\text{vdW}}$. In the asymptotic region $r \gg r_{\text{vdW}}$, both calculations reproduce the ratio $P_{[02]}^{\text{acc}} : P_{[11]}^{\text{acc}} : P_{[13]}^{\text{acc}} = 0.1875 : 0.0250 : 0.7875$ predicted by the basis transformation. However, with the decrease of r , the $P_{[SI]}^{\text{acc}}$ starts to deviate from its asymptotic value and oscillates. Except for an opposite oscillation phase, the values of $P_{[02]}^{\text{acc}}$ and $P_{[13]}^{\text{acc}}$ are rather comparable at $r < 2 r_{\text{vdW}}$, both significantly larger than that of $P_{[11]}^{\text{acc}}$. This comparison has also been extended to other species, consistently showing similar agreement between results from the reduced potentials and those from the BO potentials. Nevertheless, the r -dependent behavior of $P^{\text{acc}}[SI]$ can vary across species, particularly when $r \lesssim r_{\text{vdW}}$.

To provide further evidence that the reduced model does properly reproduce the spin structure of the real system we now analyze the case where two molecular levels are strongly coupled to each other, for instance,

in the vicinity of an avoided crossing. This scenario is shown in Figs. 5(a) and 5(b) for ^{85}Rb molecular states with $l = 0$ and 2, respectively. In both partial waves the broad avoided crossings in Fig. 5 are generated by one level in $|FM_F(f_a f_b)\rangle = |4-4(22)\rangle$ state and the other in $|4-4(33)\rangle$ state. We calculated the $|FM_F(f_a f_b)\rangle$ spin component $P_{(f_a f_b)}$ from the corresponding numerical molecular wavefunctions, $\Psi_{\text{m}}(\vec{r})$. In the vicinity of the avoided crossings for both cases, the molecular levels switch their spin state between the $|4-4(22)\rangle$ and $|4-4(33)\rangle$ state, as is shown in Fig. 7. The reduced potentials reproduce the spin structure of the relevant molecular very well throughout the whole avoided crossing, in particular for the s -wave states. For the d -wave case, the reduced potentials lead to an overall shift of about 7 G in the curves of the level energy and the spin component.

The numerical comparison so far has evidenced that our reduced potentials are a generally good replacement of the original potentials in a wide range of magnetic field regimes, despite the notable differences between the two potentials at short range. Remarkably, the reduced potentials sufficiently reproduce a variety of physical phenomena, such as the Feshbach resonance, the molecular levels avoided crossing, and the spin structure in scattering and bound molecular states. This indicates the fundamental physics governing the molecular spin structure is robust to the specific details of the short-range interactions. As we will discuss further, this understanding allows us to parameterize the complex short-range electronic spin exchange interaction, facilitating the characterization of the molecular spin structure. For deep molecular levels and those with large l , deviations appear on a quantitative level but lead to no qualitative change in concerning the physics. Nevertheless, such deviations can be mitigated by considering reduced potentials supporting a larger number of molecular states.

IV. CHARACTERIZING THE MOLECULAR SPIN STRUCTURE

In this last part of our study, we aim at characterizing the molecular spin states and reveal the underlying physics controlling their composition. In fact, the spin state of the weakly bound vdW molecules of two alkali atoms can be very different across the various atomic species. For instance, as we discussed in the previous section, weakly bound $^7\text{Li}_2$ vdW molecules are rather pure in $|FM_F(SI)\rangle$ states while those for $^{85}\text{Rb}_2$ molecules are well characterized as $|FM_F(f_a f_b)\rangle$ states. In particular circumstances, however, two $^{85}\text{Rb}_2$ molecular levels can also change into mixed states in the $|FM_F(f_a f_b)\rangle$ basis, as highlighted in the discussions of Figs. 5 and 7 near an avoided crossing. In the following we ignore such particular circumstances but rather focus on the general spin structure for a given alkali species.

To more globally characterize the molecular spin

TABLE III. Interaction and spin mixing parameters for the vdW molecules of two alkali metal atoms. See Table I for the corresponding values of r_{vdW} and E_{vdW} .

Specie	u_{st}	E_{hf}/h [MHz]	$E_{\text{hf}}/E_{\text{vdW}}$	ξ_{ex}	$\phi_{(f_a f_b)}^{\text{avg}}$	$\phi_{[SI]}^{\text{avg}}$	γ_{ex}
^7Li	0.3768	803.50	1.65	9.020	0.5685	0.9998	2336
^{23}Na	0.3096	1771.63	22.81	0.6192	0.5711	0.9909	47.11
^{39}K	0.3984	461.72	20.81	0.7968	0.5662	0.9919	53.45
^{41}K	0.1231	254.01	12.34	0.3940	0.6093	0.9867	29.45
^{85}Rb	0.0626	3035.73	481.86	0.1252	0.9728	0.7112	0.0942
^{87}Rb	0.0338	6834.68	1124.13	0.0676	0.9836	0.6232	0.0435
^{133}Cs	0.1387	9192.63	3455.86	0.2774	0.7937	0.6780	0.6408

structure for a given atomic species, we define the dimensionless spin mixing parameter

$$\gamma_{\text{ex}} \equiv (1 - \phi_{(f_a f_b)}^{\text{avg}}) / (1 - \phi_{[SI]}^{\text{avg}}). \quad (9)$$

Here, $\phi_{(f_a f_b)}^{\text{avg}}$ and $\phi_{[SI]}^{\text{avg}}$ denote the averaged "spin purity" in the $|FM_F(f_a f_b)\rangle$ and $|FM_F[SI]\rangle$ bases, respectively, given by

$$\phi_{\eta}^{\text{avg}} = \frac{1}{N} \sum_n \max_{\eta \in D} \left\{ \int_0^{\infty} \langle FM_F \eta | \Psi_m^n(r) \rangle^2 d^3 \vec{r} \right\}, \quad (10)$$

where $\eta = (f_a f_b)$ or $[SI]$ and D is the corresponding variable domain of η . In Eq. (10) we extract the dominant spin component value of each molecular state n in the $|FM_F \eta\rangle$ basis and average them over the total number N of molecular states included in the reduced potentials. (A similar procedure could be performed on the molecular states of the BO potentials by restricting the range of energies of such states.) In this work, we consider $N \approx 80$ -200 states across the species, counting for molecular levels of all partial waves and binding energies up to a few thousands of E_{vdW} . According to Eq. (9), $\gamma_{\text{ex}} \ll 1$ implies that the considered molecular states are purely $|FM_F(f_a f_b)\rangle$ while for $\gamma_{\text{ex}} \gg 1$ the molecular states are purely $|FM_F[SI]\rangle$, and any number in between indicates the degree of molecular spin mixing. The values for γ_{ex} and the averaged spin purities in the two bases are listed in Table III. We find that $\gamma_{\text{ex}} \ll 1$ for ^{87}Rb and ^{85}Rb , while the $\gamma_{\text{ex}} \gg 1$ for ^7Li , ^{23}Na , ^{39}K and ^{41}K . We note, however, that for ^{133}Cs $\gamma_{\text{ex}} \sim 1$, indicating that the Cs_2 molecular states are mixed in both $|FM_F(f_a f_b)\rangle$ and $|FM_F[SI]\rangle$ bases.

At zero magnetic field, the spin structure of alkali diatomic vdW molecules fundamentally originates from the competition between the electronic spin exchange and hyperfine interactions. In general, in cases where electronic spin exchange interaction is dominant over hyperfine interaction molecular states are well characterized as a $|FM_F[SI]\rangle$ state. On the other hand, for cases where the hyperfine interaction is dominant over electronic spin exchange interaction molecular states are instead of $|FM_F(f_a f_b)\rangle$ character. Evidently, in the case where there is a balance between these two interactions,

the molecular states can be mixed in both $|FM_F[SI]\rangle$ and $|FM_F(f_a f_b)\rangle$ basis. In the following, we aim to gain a deeper understanding of our numerical results on the spin mixing parameter γ_{ex} of vdW molecules by characterizing both electronic exchange and hyperfine interactions. We shall focus on a simple, and physically intuitive, picture for qualitative understanding.

A. Effective electronic spin exchange interaction

The electronic spin exchange interaction corresponds to the difference between singlet and triplet potentials which depends on r , which is prominent at short-range. Its actual form can be complex and can vary significantly across atomic species. Nevertheless, our comparative analysis indicates that the molecular spin structure is insensitive to the specific details of the interatomic interaction at short range. Largely different potential models that share the same singlet and triplet scattering lengths or bound levels provide comparable descriptions of the spin structure in weakly bound molecules. This motivates us to effectively parameterize the complex short-range electronic spin exchange interaction using the energy splittings between singlet and triplet levels, which result from the electronic spin exchange interaction. Specifically, we will define an effective electronic spin exchange interaction for a given vdW molecular state as the energy difference between adjacent singlet and triplet levels. We focus on s -wave vdW molecular states.

For vdW interactions, molecular levels can be classified according to their location within a given universal energy range for each vibrational quantum number v of a given partial wave l [45, 46]. For instance, for $l = 0$, the $v = -1$ level is always within a energy range of $[-39.5, 0] E_{\text{vdW}}$ while the $v = -2$ level is within $[-272.5, -39.5] E_{\text{vdW}}$. These universal energy intervals are referred to as "vdW energy bins" [45] and are illustrated in Fig. 2 by the different colored regions. According to quantum defect theory [46], for vdW interactions the location of the energy of an s -wave level in a given energy bin can be characterized in terms of the physical scattering lengths

(a_s or a_t), through the quantity u defined as [54]

$$u(a) = \tan^{-1}[\bar{a}/(a - \bar{a})]/\pi, \quad (11)$$

where a denotes the scattering length of the associated interaction potentials and $\bar{a} \approx 0.9560 r_{\text{vdW}}$, the mean scattering length [55]. For $a \rightarrow \pm\infty$, u approaches zero and the ($v = -1$) bound level approaches the potential threshold (i.e., the upper boundary of the first bin) while the energy of additional more deeply bound molecular states approach the other boundaries of the energy bins. For finite values of a , u is non-zero and characterizes the distance of the bound levels from such a boundary. Figure 8 illustrates the behavior of the bound levels in the first three energy bins with a varying a tuned by the short-range parameter λ for the Lennard-Jones potential $V_{LJ}(r) = -C_6/r^6(1 - \lambda^6/r^6)$. This figure clearly shows that the bound levels appear at the boundaries of the bins when $a \rightarrow \pm\infty$, while moving away from the boundaries when a is finite.

Based on the discussion above, the energy separation of nearby singlet and triplet levels, and consequently the effective electronic spin exchange interaction, can be characterized by $|u(a_s) - u(a_t)| \in [0, 1]$. We note that $|u(a_s) - u(a_t)|$ will properly parameterize the energy difference between nearby singlet and triplet levels whenever they are in the same energy bin or adjacent bins. A concrete example of the latter is $^{85}\text{Rb}_2$ in Fig. 2, in which $|u(a_s) - u(a_t)| = 0.06$ characterized properly the small energy difference between a singlet level at the top of one bin and a triplet level at the bottom of the adjacent bin from above. However, the energy separation of nearby singlet and triplet levels are not fairly described by $|u(a_s) - u(a_t)|$ when the values for a_s and a_t are close to each other but with one slightly smaller and the other slightly larger than \bar{a} . This problem can be resolved by defining $u_{st} = \min(|u(a_s) - u(a_t)|, 1 - |u(a_s) - u(a_t)|) \in [0, 1/2]$. The values of u_{st} for different atomic species we study here are listed in Table III. These values are generally consistent with the energy separation of singlet and triplet levels in Fig. 2. As a result, for the i th energy bin, the quantity

$$\tilde{E}_{\text{ex}}^{(i)} = u_{st} E_{\text{bin}}^{(i)}, \quad (12)$$

will provide a measure of the effective electronic spin-exchange interaction, as a simple alternative to the actual energy difference between nearby singlet and triplet levels, $\Delta E_{st}^{(i)}$, calculated numerically for a given potential model. In Fig. 9, we use the energies from the BO potentials to demonstrate that $\tilde{E}_{\text{ex}}^{(i)}$ is a fairly good approximation to $\Delta E_{st}^{(i)}$. This validates the use of $\tilde{E}_{\text{ex}}^{(i)}$ to characterize the effective exchange interaction of a given energy bin.

B. Effective hyperfine interaction

In order to characterize the effective hyperfine interaction we follow a similar approach to that of the

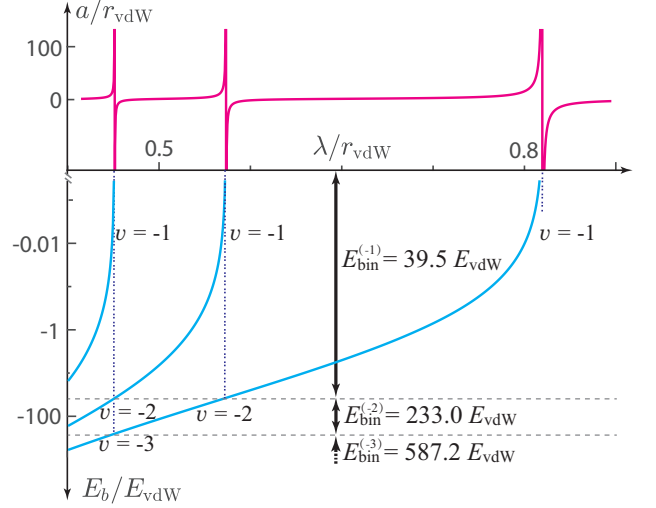


FIG. 8. The scattering length and bound-state energies of a Lennard-Jones potential are tuned by the short-range parameter λ . The horizontal solid lines represent the boundaries of vdW energy bins. The dotted vertical lines indicate that vdW bound levels approach these boundaries when the two-body scattering length diverges.

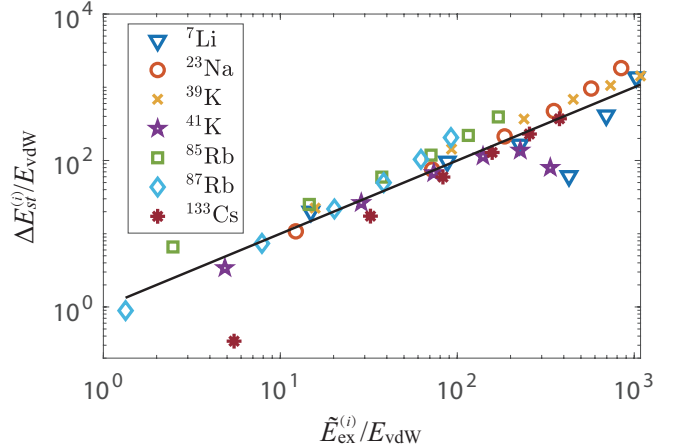


FIG. 9. The energy difference of the nearby singlet and triplet levels $\Delta E_{st}^{(i)}$ versus $\tilde{E}_{\text{ex}}^{(i)}$ in the first six energy bins. The solid line marks where $\Delta E_{st}^{(i)} = \tilde{E}_{\text{ex}}^{(i)}$.

electronic spin exchange interaction. Now we focus on the energy difference between nearby molecular states in the presence of the hyperfine interaction. We consider a given molecular level in the ground hyperfine state $|FM_F(f_a f_b)\rangle = |2f^*, -2f^*(f^* f^*)\rangle$ as a reference. The energy of the corresponding molecular levels of the excited hyperfine state will be shifted upwards by, approximately, the hyperfine splitting constant $E_{\text{hf}} = 2(f^* + 1)A_{\text{hf}}$ if one atom is in the excited $f^* + 1$ state, or $2E_{\text{hf}}$ in the case that both atoms are in the $f^* + 1$ state. Based on this, one could intuitively characterize effective hyperfine interaction from the energy difference

of nearby hyperfine molecular levels, E_{hf} . This, however, is valid only if E_{hf} is small comparable to the energy bin so that the original and the shifted energy levels are still in the same energy bin. Nevertheless, in some cases the hyperfine interaction can shift a level into a different energy bin if E_{hf} is large enough and the energy difference of nearby hyperfine molecular levels is not simply E_{hf} or $2E_{\text{hf}}$. Instead, it is restricted to the size of the corresponding energy bin with an upper bound given, roughly, by $E_{\text{bin}}/2$. Therefore, as a more precise characterization of the energy separation is not straightforwardly available, we will utilize this upper bound for a rough characterization of the effect of the hyperfine interaction. Taking both cases into account, we use the quantity

$$\tilde{E}_{\text{hf}}^{(i)} = \min(E_{\text{hf}}, E_{\text{bin}}^{(i)}/2), \quad (13)$$

to characterize the effective hyperfine interaction in the i th energy bin. The values for E_{hf} for different atomic species we study here are listed in Table III.

C. The exchange parameter

According to the above analysis, we can now define the dimensionless exchange parameter as a ratio between effective electronic spin exchange and effective hyperfine interactions

$$\xi_{\text{ex}}^{(i)} = \frac{\tilde{E}_{\text{ex}}^{(i)}}{\tilde{E}_{\text{hf}}^{(i)}} = \frac{u_{st} E_{\text{bin}}^{(i)}}{\min(E_{\text{hf}}, E_{\text{bin}}^{(i)}/2)} \quad (14)$$

to estimate the relative strength of the electronic spin exchange for vdW molecules. This definition for $\xi_{\text{ex}}^{(i)}$ depends on the energy bin i in which the molecular states are located when used to characterize the spin structure of the corresponding molecular states. Figure 10 shows that the value of $\xi_{\text{ex}}^{(i)}$ increases with the bin index i for ${}^7\text{Li}$, ${}^{23}\text{Na}$, ${}^{39}\text{K}$ and ${}^{41}\text{K}$ while for heavier species ${}^{85}\text{Rb}$, ${}^{87}\text{Rb}$ and ${}^{133}\text{Cs}$ such bin-dependency is rather weak, particularly in the first few bins relevant to our present study. Nevertheless, the values of $\xi_{\text{ex}}^{(i)}$ s across different species preserve the same order from the first bin down to the 5th bin, with relative values consistent to those of γ_{ex} . For deeper bins, the order switches only between ${}^{85}\text{Rb}$ and ${}^{133}\text{Cs}$. This demonstrates the qualitative agreement between our simple parameter $\xi_{\text{ex}}^{(i)}$ and the numerical results γ_{ex} to characterize the spin structure of vdW molecules. For instance, in the cases of strong spin exchange ($\xi_{\text{ex}}^{(i)} \gg 1$), as is the case of ${}^7\text{Li}$, we also obtain $\gamma_{\text{ex}} \gg 1$, for weak spin exchange species ${}^{85}\text{Rb}$ and ${}^{87}\text{Rb}$, we find both $\xi_{\text{ex}}^{(i)} \ll 1$ and $\gamma_{\text{ex}} \ll 1$, while for intermediate spin exchange species, like ${}^{133}\text{Cs}$, we also have $\xi_{\text{ex}} \sim 1$ and $\gamma_{\text{ex}} \sim 1$. It should be noted that using \tilde{E}_{hf} instead of E_{hf} in the definition of $\xi_{\text{ex}}^{(i)}$ is crucial for explaining the γ_{ex} for ${}^{133}\text{Cs}$. For ${}^{23}\text{Na}$, ${}^{39}\text{K}$

and ${}^{41}\text{K}$ atoms, the corresponding vdW molecules evolve from the intermediate to a strong spin exchange regime with the increase of bin index i . We also emphasize here the advantage that $\xi_{\text{ex}}^{(i)}$ can reveal the physical origin of the molecular spin property based on fundamental atomic and interatomic interactions. In Table III, we list the minimal value of $\xi_{\text{ex}}^{(i)}$ (i.e. that of the first bin) with the superscript omitted. This value is used in the analysis presented in Ref. [32].

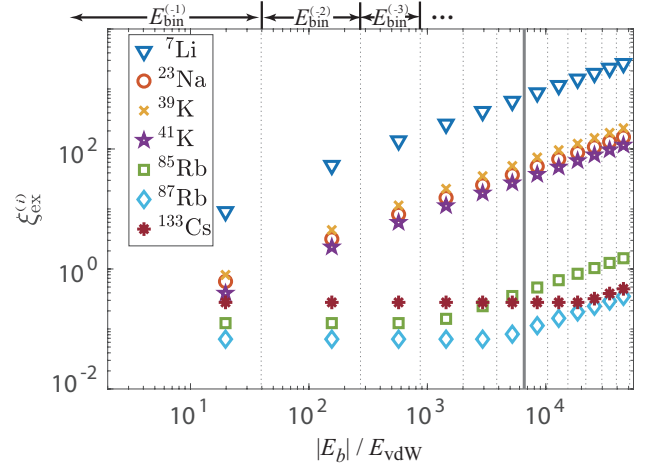


FIG. 10. ξ_{ex} versus vdW energy bins. The data points of each bin are placed at the corresponding middle value of $|E_b|$. The vertical lines indicate the boundaries of the bins. The right boundary of the sixth energy bin is highlighted as it is the binding energy regime covered by our reduced potential models (except for that for ${}^{133}\text{Cs}$).

V. CONCLUSION AND OUTLOOK

In summary, we have studied the weakly bound van der Waals molecules of ${}^7\text{Li}_2$, ${}^{23}\text{Na}_2$, ${}^{39}\text{K}_2$, ${}^{41}\text{K}_2$, ${}^{85}\text{Rb}_2$, ${}^{87}\text{Rb}_2$ and ${}^{133}\text{Cs}_2$, with a focus on determining and understanding their binding energies and spin structures. For each atomic species, we constructed reduced singlet and triplet potentials to replace the original Born-Oppenheimer potentials. The reduced potentials support typically only 5 ~ 7 s -wave bound states and are more suitable for numerical simulations of various three-body problems. We show that they can reproduce well the physical properties of two-atom scattering and molecular states in the presence of a magnetic field, such as the scattering length, the scattering effective range and the molecular binding energy as well as the spin structure of scattering and molecular wavefunctions. At zero magnetic field, we define the quantity γ_{ex} to characterize the molecular spin structure by using the averaged spin purity in two different bases, obtained directly from the numerical simulations for each atomic species. The result of γ_{ex} across alkali species characterizes the competition between the electronic spin exchange

and the hyperfine interactions. For van der Waals molecules, we define a simple parameter ξ_{ex} , which is a function of the singlet and triplet scattering lengths, the atomic hyperfine splitting constant, and the size of the energy bin for a given molecular level. We find that ξ_{ex} captures qualitatively the competition between the effective electronic spin exchange and hyperfine interactions and explains fairly well the numerical result of γ_{ex} .

For future studies, the characterization of spin structure of vdW molecules can be extended to a finite magnetic field to include the Zeeman interaction. The understanding of vdW molecules that we have gained here can be applied to explore the underlying mechanisms of reactions that involve these molecules. The result of the present work has been already applied in our studies on the spin hierarchy in the product state distribution of three-body recombination [32] and on controlling three-body recombination reaction via a Feshbach resonance [51]. Further studies on the control of the three-body recombination via the spin mixing of product molecular state as well as on ultracold state-to-state atom-vdW molecule reactions are underway.

This work was supported by the Baden-Württemberg Stiftung through the Internationale Spitzenforschung program (BWST, contract No. ISF2017-061) and by the German Research Foundation (DFG, Deutsche Forschungsgemeinschaft, contract No. 399903135). We acknowledge support from bwForCluster JUSTUS 2 for high performance computing. J.P.D. also acknowledges partial support from the U.S. National Science Foundation (PHY-2012125 and PHY-2308791) and NASA/JPL (1502690).

Appendix A: Molecular spin basis

Following standard quantum mechanics, the two molecular bases $|FM_F(f_a f_b)\rangle$ and $|FM_F[SI]\rangle$ can be expressed as

$$|FM_F(f_a f_b)\rangle = \sum_{m_{f_a} m_{f_b}} C_{f_a m_{f_a} f_b m_{f_b}}^{FM_F} |f_a m_{f_a}\rangle |f_b m_{f_b}\rangle, \quad (\text{A1})$$

and

$$|FM_F[SI]\rangle = \sum_{M_I M_S} C_{SM_S IM_I}^{FM_F} |SM_S\rangle |IM_I\rangle, \quad (\text{A2})$$

respectively, where $C_{j_1 m_1 j_2 m_2}^{j_3 m_3}$ is the Clebsch-Gordan coefficient. We use M_S and M_I to denote the projection quantum number of the molecular total electronic and nuclear spins, respectively.

The $|FM_F(f_a f_b)\rangle$ basis is connected to the $|FM_F[SI]\rangle$ basis via a 9- j symbol

$$|FM_F(f_a f_b)\rangle = \sum_{S, I} \sqrt{2f_a + 1} \sqrt{2f_b + 1} \sqrt{2S + 1} \sqrt{2I + 1} \\ \times \sqrt{2 - \delta_{f_a f_b}} \begin{Bmatrix} s_a & s_b & S \\ i_a & i_b & I \\ f_a & f_b & F \end{Bmatrix} |FM_F[SI]\rangle. \quad (\text{A3})$$

Applying Eq. (A3) to our investigation of ${}^7\text{Li}$ gives the expression of the initial state of the reacting atomic pair

$$|2\text{-}2(11)\rangle = \frac{\sqrt{3}}{4} |2\text{-}2[02]\rangle - \frac{1}{2\sqrt{10}} |2\text{-}2[11]\rangle + \frac{3\sqrt{7}}{4\sqrt{5}} |2\text{-}2[13]\rangle, \quad (\text{A4})$$

which leads to the ratio of the initial components in $|2\text{-}2[02]\rangle$, $|2\text{-}2[11]\rangle$ and $|2\text{-}2[13]\rangle$

$$\left| \frac{\sqrt{3}}{4} \right|^2 : \left| -\frac{1}{2\sqrt{10}} \right|^2 : \left| \frac{3\sqrt{7}}{4\sqrt{5}} \right|^2 = 0.1875 : 0.0250 : 0.7875, \quad (\text{A5})$$

respectively.

-
- [1] B. Jeziorski, R. Moszynski, and K. Szalewicz, Perturbation Theory Approach to Intermolecular Potential Energy Surfaces of van der Waals Complexes, *Chemical Reviews* **94**, 1887 (1994).
- [2] A. M. Reilly and A. Tkatchenko, Van der Waals dispersion interactions in molecular materials: beyond pairwise additivity, *Chem. Sci.* **6**, 3289 (2015).
- [3] B. L. Blaney and G. E. Ewing, Van Der Waals Molecules, *Annual Review of Physical Chemistry* **27**, 553 (1976).
- [4] E. R. Bernstein, Dynamics and Photochemistry of Neutral van der Waals Clusters, *Annual Review of Physical Chemistry* **46**, 197 (1995), pMID: 24329404.
- [5] K. M. Jones, E. Tiesinga, P. D. Lett, and P. S. Julienne, Ultracold photoassociation spectroscopy: Long-range molecules and atomic scattering, *Rev. Mod. Phys.* **78**, 483 (2006).
- [6] D. J. Nesbitt, Toward state-to-state dynamics in ultracold collisions: Lessons from high-resolution spectroscopy of weakly bound molecular complexes, *Chemical Reviews* **112**, 5062 (2012), pMID: 22937828.
- [7] J. Hermann, R. A. J. DiStasio, and A. Tkatchenko, First-Principles Models for van der Waals Interactions in Molecules and Materials: Concepts, Theory, and Applications, *Chemical Reviews* **117**, 4714 (2017), pMID: 28272886.
- [8] J. M. Hutson, Intermolecular Forces from the Spectroscopy of Van Der Waals Molecules, *Annual Review of Physical Chemistry* **41**, 123 (1990).
- [9] J. Koperski, Study of diatomic van der Waals complexes in supersonic beams, *Physics Reports* **369**, 177 (2002).
- [10] G. A. Rance, D. H. Marsh, S. J. Bourne, T. J. Reade, and A. N. Khlobystov, van der Waals Interactions between Nanotubes and Nanoparticles for Controlled Assembly of Composite Nanostructures, *ACS Nano* **4**, 4920 (2010), pMID: 20684572.
- [11] V. V. Gobre and A. Tkatchenko, Scaling laws for van der Waals interactions in nanostructured materials, *Nature Communications* **4**, 2341 (2013).
- [12] C. A. S. Batista, R. G. Larson, and N. A. Kotov, Nonadditivity of nanoparticle interactions, *Science* **350**, 1242477 (2015).
- [13] B. A. Persson, B. Jönsson, and M. Lund, Enhanced Protein Steering: Cooperative Electrostatic and van der Waals Forces in Antigen-Antibody Complexes, *The Journal of Physical Chemistry B* **113**, 10459 (2009), pMID: 19583233.
- [14] M. Rossi, W. Fang, and A. Michaelides, Stability of Complex Biomolecular Structures: van der Waals, Hydrogen Bond Cooperativity, and Nuclear Quantum Effects, *The Journal of Physical Chemistry Letters* **6**, 4233 (2015), pMID: 26722963.
- [15] J. P. Toennies and A. F. Vilesov, Superfluid helium droplets: A uniquely cold nanomatrix for molecules and molecular complexes, *Angewandte Chemie International Edition* **43**, 2622 (2004).
- [16] K. Szalewicz, Interplay between theory and experiment in investigations of molecules embedded in superfluid helium nanodroplets[†], *International Reviews in Physical Chemistry* **27**, 273 (2008).
- [17] N. Tariq, N. A. Taisan, V. Singh, and J. D. Weinstein, Spectroscopic Detection of the LiHe Molecule, *Phys. Rev. Lett.* **110**, 153201 (2013).
- [18] N. Brahms, T. V. Tscherbul, P. Zhang, J. Klos, H. R. Sadeghpour, A. Dalgarno, J. M. Doyle, and T. G. Walker, Formation of van der Waals Molecules in Buffer-Gas-Cooled Magnetic Traps, *Phys. Rev. Lett.* **105**, 033001 (2010).
- [19] N. Brahms, T. V. Tscherbul, P. Zhang, J. Klos, R. C. Forrey, Y. S. Au, H. R. Sadeghpour, A. Dalgarno, J. M. Doyle, and T. G. Walker, Formation and dynamics of van der Waals molecules in buffer-gas traps, *Phys. Chem. Chem. Phys.* **13**, 19125 (2011).
- [20] N. Quiros, N. Tariq, T. V. Tscherbul, J. Klos, and J. D. Weinstein, Cold Anisotropically Interacting van der Waals Molecule: TiHe, *Phys. Rev. Lett.* **118**, 213401 (2017).
- [21] M. Mirahmadi and J. Pérez-Ríos, On the formation of van der Waals complexes through three-body recombination, *The Journal of Chemical Physics* **154**, 034305 (2021).
- [22] M. Mirahmadi and J. Pérez-Ríos, Classical threshold law for the formation of van der Waals molecules, *The Journal of Chemical Physics* **155**, 094306 (2021).
- [23] T. Köhler, K. Góral, and P. S. Julienne, Production of cold molecules via magnetically tunable feshbach resonances, *Rev. Mod. Phys.* **78**, 1311 (2006).
- [24] J. Ulmanis, J. Deiglmayr, M. Repp, R. Wester, and M. Weidemüller, Ultracold molecules formed by photoassociation: Heteronuclear dimers, inelastic collisions, and interactions with ultrashort laser pulses, *Chemical Reviews* **112**, 4890 (2012), pMID: 22931226.
- [25] A. Härter, A. Krüchow, M. Deiß, B. Drews, E. Tiemann, and J. Hecker Denschlag, Population distribution of product states following three-body recombination in an ultracold atomic gas, *Nature Physics* **9**, 512 (2013).
- [26] J. P. D’Incao, Few-body physics in resonantly interacting ultracold quantum gases, *Journal of Physics B: Atomic, Molecular and Optical Physics* **51**, 043001 (2018).
- [27] J. Wolf, M. Deiß, A. Krüchow, E. Tiemann, B. P. Ruzic, Y. Wang, J. P. D’Incao, P. S. Julienne, and J. Hecker Denschlag, State-to-state chemistry for three-body recombination in an ultracold rubidium gas, *Science* **358**, 921 (2017).
- [28] J. Wolf, M. Deiß, and J. Hecker Denschlag, Hyperfine Magnetic Substate Resolved State-to-State Chemistry, *Phys. Rev. Lett.* **123**, 253401 (2019).
- [29] S. Haze, J. P. D’Incao, D. Dorer, M. Deiß, E. Tiemann, P. S. Julienne, and J. Hecker Denschlag, Spin-Conservation Propensity Rule for Three-Body Recombination of Ultracold Rb Atoms, *Phys. Rev. Lett.* **128**, 133401 (2022).
- [30] S. Haze, J. P. D’Incao, D. Dorer, J.-L. Li, M. Deiß, E. Tiemann, P. S. Julienne, and J. Hecker Denschlag, Energy scaling of the product state distribution for three-body recombination of ultracold atoms, *Phys. Rev. Res.* **5**, 013161 (2023).
- [31] J.-L. Li, T. Secker, P. M. A. Mestrom, and S. J. J. M. F. Kokkelmans, Strong spin-exchange recombination of three weakly interacting ⁷Li atoms, *Phys. Rev. Res.* **4**, 023103 (2022).
- [32] J.-L. Li, P. S. Julienne, J. Hecker Denschlag, and J. P. D’Incao, Spin hierarchy in van der Waals molecule formation via ultracold three-body recombination (2024),

- arXiv:2407.18567 [physics.atom-ph].
- [33] P. S. Julienne and J. M. Hutson, Contrasting the wide Feshbach resonances in ${}^6\text{Li}$ and ${}^7\text{Li}$, *Phys. Rev. A* **89**, 052715 (2014).
- [34] S. Knoop, T. Schuster, R. Scelle, A. Trautmann, J. Appmeier, M. K. Oberthaler, E. Tiesinga, and E. Tiemann, Feshbach spectroscopy and analysis of the interaction potentials of ultracold sodium, *Phys. Rev. A* **83**, 042704 (2011).
- [35] E. Tiemann, P. Gersema, K. K. Voges, T. Hartmann, A. Zenesini, and S. Ospelkaus, Beyond Born-Oppenheimer approximation in ultracold atomic collisions, *Phys. Rev. Res.* **2**, 013366 (2020).
- [36] C. Strauss, T. Takekoshi, F. Lang, K. Winkler, R. Grimm, J. Hecker Denschlag, and E. Tiemann, Hyperfine, rotational, and vibrational structure of the $a^3\Sigma_u^+$ state of ${}^{87}\text{Rb}_2$, *Phys. Rev. A* **82**, 052514 (2010).
- [37] M. Berninger, A. Zenesini, B. Huang, W. Harm, H.-C. Nägerl, F. Ferlaino, R. Grimm, P. S. Julienne, and J. M. Hutson, Feshbach resonances, weakly bound molecular states, and coupled-channel potentials for cesium at high magnetic fields, *Phys. Rev. A* **87**, 032517 (2013).
- [38] Three-body simulation is not only essential for three-body recombination but also necessary for the reaction of a vdW molecule and an atom because the vdW bond is very loose.
- [39] Y. Wang and P. S. Julienne, Universal van der Waals physics for three cold atoms near Feshbach resonances, *Nature Physics* **10**, 768 (2014).
- [40] R. Chapurin, X. Xie, M. J. Van de Graaff, J. S. Popowski, J. P. D’Incao, P. S. Julienne, J. Ye, and E. A. Cornell, Precision test of the limits to universality in few-body physics, *Phys. Rev. Lett.* **123**, 233402 (2019).
- [41] K.-M. Tempest and S. Jonsell, Multichannel hyperspherical model for Efimov physics with van der Waals interactions controlled by a Feshbach resonance, *Phys. Rev. A* **107**, 053319 (2023).
- [42] T. Secker, J.-L. Li, P. M. A. Mestrom, and S. J. J. M. F. Kokkelmans, Multichannel nature of three-body recombination for ultracold ${}^{39}\text{K}$, *Phys. Rev. A* **103**, 022825 (2021).
- [43] J. van de Kraats, D. J. M. Ahmed-Braun, J.-L. Li, and S. J. J. M. F. Kokkelmans, Emergent Inflation of the Efimov Spectrum under Three-Body Spin-Exchange Interactions, *Phys. Rev. Lett.* **132**, 133402 (2024).
- [44] E. Arimondo, M. Inguscio, and P. Violino, Experimental determinations of the hyperfine structure in the alkali atoms, *Rev. Mod. Phys.* **49**, 31 (1977).
- [45] C. Chin, R. Grimm, P. Julienne, and E. Tiesinga, Feshbach resonances in ultracold gases, *Rev. Mod. Phys.* **82**, 1225 (2010).
- [46] B. Gao, Zero-energy bound or quasibound states and their implications for diatomic systems with an asymptotic van der Waals interaction, *Phys. Rev. A* **62**, 050702 (2000).
- [47] D. E. Manolopoulos, An improved log derivative method for inelastic scattering, *The Journal of Chemical Physics* **85**, 6425 (1986).
- [48] K. Willner, O. Dulieu, and F. Masnou-Seeuws, Mapped grid methods for long-range molecules and cold collisions, *The Journal of Chemical Physics* **120**, 548 (2004).
- [49] X. Xie, M. J. Van de Graaff, R. Chapurin, M. D. Frye, J. M. Hutson, J. P. D’Incao, P. S. Julienne, J. Ye, and E. A. Cornell, Observation of Efimov Universality across a Nonuniversal Feshbach Resonance in ${}^{39}\text{K}$, *Phys. Rev. Lett.* **125**, 243401 (2020).
- [50] R. J. Wild, P. Makotyn, J. M. Pino, E. A. Cornell, and D. S. Jin, Measurements of Tan’s Contact in an Atomic Bose-Einstein Condensate, *Phys. Rev. Lett.* **108**, 145305 (2012).
- [51] S. Haze, J.-L. Li, D. Dorer, J. P. D’Incao, P. S. Julienne, E. Tiemann, M. Deiß, and J. Hecker Denschlag, Controlling few-body reaction pathways using a Feshbach resonance (2024), arXiv:2408.14922 [cond-mat.quant-gas].
- [52] Y. Wang, J. P. D’Incao, and C. H. Greene, Efimov effect for three interacting bosonic dipoles, *Phys. Rev. Lett.* **106**, 233201 (2011).
- [53] Y. Wang, J. P. D’Incao, and C. H. Greene, Universal three-body physics for fermionic dipoles, *Phys. Rev. Lett.* **107**, 233201 (2011).
- [54] H. Friedrich and J. Trost, Working with WKB waves far from the semiclassical limit, *Physics Reports* **397**, 359 (2004).
- [55] V. V. Flambaum, G. F. Gribakin, and C. Harabati, Analytical calculation of cold-atom scattering, *Phys. Rev. A* **59**, 1998 (1999).